Transcript processing and export kinetics are rate-limiting steps in expressing vertebrate segmentation clock genes

Nathaniel P. Hoyle[1] and David Ish-Horowicz[2]

Cancer Research UK Developmental Genetics Laboratory, London Research Institute, London WC2A 3LY, United Kingdom

Edited by Clifford J. Tabin, Harvard Medical School, Boston, MA, and approved September 16, 2013 (received for review May 12, 2013)

Sequential production of body segments in vertebrate embryos is regulated by a molecular oscillator (the segmentation clock) that drives cyclic transcription of genes involved in positioning intersegmental boundaries. Mathematical modeling indicates that the period of the clock depends on the total delay kinetics of a negative feedback circuit, including those associated with the synthesis of transcripts encoding clock components [Lewis J (2003) *Curr Biol* 13(16):1398–1408]. Here, we measure expression delays for three transcripts [*Lunatic fringe*, *Hes7*/*her1*, and *Notch-regulated-ankyrin-repeat-protein* (*Nrarp*)], that cycle during segmentation in the zebrafish, chick, and mouse, and provide in vivo measurements of endogenous splicing and export kinetics. We show that mRNA splicing and export are much slower than transcript elongation, with the longest delay (about 16 min in the mouse) being due to mRNA export. We conclude that the kinetics of mRNA and protein production and destruction can account for much of the clock period, and provide strong support for delayed autorepression as the underlying mechanism of the segmentation clock.

transcriptional delays | RNA export | RNA splicing | mRNA processing | somites

Production of reiterated vertebrate structures is regulated by an oscillator (the segmentation clock), proposed in 1976 (1) and first visualized as driving cyclic transcription in the presomitic mesoderm (PSM), a zone of unsegmented cells from which epithelial balls of tissue, the somites, bud off and generate repetitive axial structures, such as the vertebrae, ribs, and skeletal muscles (2–4). According to this "clock-and-wavefront" mechanism, cells advance through the PSM until they encounter a differentiation wavefront that causes the clock to slow down and freeze. As neighboring clocks are synchronized via Notch signaling, the cyclic transcript pattern appears as a kinematic wave traveling anteriorly through the PSM once per clock cycle (5–7).

Central to current models of the segmentation clock is the idea of delayed negative-feedback loops whose period of oscillation is determined by the delay kinetics of individual steps in the loop (8). In the simplest model, a gene represses its own transcription directly, and the period of the cycle is largely governed by delays inherent to the production of competent repressive protein (i.e., the times taken to produce a functional transcript, to translate an active protein, to initiate repression, and to degrade the mRNA and protein) (8). This model is sufficient to account for oscillatory expression of the *her1*/*her7* genes, which encode redundant Hairy/Hes-related transcriptional repressors, in the zebrafish PSM.

Several negative-feedback loops can cycle within the PSM, most notably in the Notch, Wnt, and FGF signaling pathways. The *hairy*-related Notch target genes cycle not just in the zebrafish (*her1*/*her7*) but in the mouse (*Hes7*) and chick (*c-hairy1*/*Her1*), and appear to autorepress their own expression either directly or indirectly. Ectopic expression of *her1* and *her7* in zebrafish embryos represses endogenous expression of *her1* and *her7* (9), and the *Hes7* promoter is ectopically activated in *Hes7*$^{-/-}$ mice (10). Notch signaling also oscillates (11, 12), and may regulate its own activity via *Lunatic fringe* (*Lfng*), which cycles in the chick and mouse PSM, and encodes a glycosyl-transferase that posttranslationally inhibits the activity of the Notch receptor (13, 14). *Hes7* and *Lfng* are both required for normal somite formation; mouse mutations in either gene disrupt clock output and segmentation (10, 15). Evidence of negative regulation of Wnt and FGF signaling comes from cyclic expression in the mouse and chick of the negative Wnt regulators Axin2 and Dkk1, as well as the FGF inhibitors Sprouty-2 and Sprouty-4 and Dusp-4 and Dusp-6 (16).

It is unclear which of these pathways contribute to determining the pace of the clock, although dynamic Notch signaling is evolutionarily conserved in animals undergoing progressive segmentation (16, 17). It is also not known how species-specific differences in clock period (e.g., 30 min in zebrafish, 90 min in chick, and 120 min in mouse) arise.

To understand how the clock works, we need to identify both its circuitry and the delays in the circuit. Protein translation is very rapid (18, 19), and thus is unlikely to affect clock period significantly. However, production of mature transcripts is slower and more likely to contribute to clock period. Lewis and colleagues (9) have estimated that *her1* is subject to a total transcript delay of 5 min in the zebrafish PSM, which is consistent with the kinetic constraints required for a 30-min clock period. However, the zebrafish segmentation clock oscillates particularly quickly, and so may differ mechanistically from slower clocks, such as those in the chick or mouse.

Estimates of transcript elongation rates in vertebrates have varied greatly among different systems (0.7–4.3 kb/min) (20) and have usually relied on ex vivo analysis of gene expression, often of unusually long or synthetic genes in cultured cells. Recent measurements have converged toward a mean rate of 3.1–4 kb/min

Significance

This paper describes in vivo measurements of the kinetics of transcript processing and export for endogenous genes in mouse and chick embryos. It shows that transcript export is unexpectedly slow, even slower than splicing, and relates its finding to rate-limiting steps that would contribute to the molecular oscillator that drives segmentation in vertebrate embryos. It also relates them to interspecies differences in clock period.

Author contributions: N.P.H. and D.I.-H. designed research; N.P.H. performed research; N.P.H. analyzed data; and N.P.H. and D.I.-H. wrote the paper.

The authors declare no conflict of interest.

This article is a PNAS Direct Submission.

Freely available online through the PNAS open access option.

[1]Present address: Medical Research Council Laboratory of Molecular Biology, Cambridge Biomedical Campus, Cambridge CB2 0QH, United Kingdom.

[2]To whom correspondence should be addressed. E-mail: david.horowicz@cancer.org.uk.

This article contains supporting information online at www.pnas.org/lookup/suppl/doi:10.1073/pnas.1308811110/-/DCSupplemental.

in cultured mammalian cells (21–25), and an elongation rate of 4.8 kb/min has been measured in zebrafish embryos (26).

Less is known about the kinetics of mRNA processing and export. Ex vivo measurements measured splicing delays in human cells of 5–10 min independent of intron lengths (24), and the kinetics of exporting nuclear mRNA into the cytoplasm have been estimated to range between 5 and 30 min depending on messenger RNP diffusion coefficients and nuclear environment (21, 27, 28).

The periodicity of oscillatory expression of *Hes1* in mouse cultured cells matches that of *Hes* gene expression in the PSM (29), suggesting that ex vivo transcript kinetics also apply in vivo and that posttranscriptional delays in mRNA production might have a profound impact on the clock circuitry. Intron delays can be important for engineered feedback loops (30), and splicing delays seem to be critical for segmentation periodicity in the mouse (31).

In this paper, we measure the transcript kinetics of several endogenous segmentation genes in zebrafish, chick, and mouse embryos. Using a combination of quantitative RT-PCR (qRT-PCR) in cell culture and in vivo time-correlated FISH, we show that delays due to transcriptional elongation of cycling Notch pathway genes are brief. We find that mRNA splicing, and maturation and nuclear export in particular, are rate-limiting in generating functional transcripts and increase with the clock period in the different species.

Results

Transcript Kinetics of *Lfng* and *Hes7* in Cultured Cells. The clock period varies widely among different animals, presumably due to interspecies differences in circuit kinetics. To provide a quantitative basis for transcriptional delays that might contribute to negative-feedback models of the segmentation clock, we examined two Notch pathway genes, *Lfng* and *Hes7*, that cycle in the PSM during segmentation.

We initially measured the kinetics in stable mouse C3H10T1/2 cell lines containing hormone-inducible constructs driving expression of mouse *Lfng* or *Hes7* primary transcripts (*Materials and Methods*). Following induction, nuclear and cytoplasmic accumulation of various RNA regions was monitored using qRT-PCR. We determined elongation and splicing kinetics by amplifying primary or spliced RNAs with appropriate exon, intron, and junction-spanning primers, and we compared nuclear and cytoplasmic fractions to calculate postsplicing delays (which we refer to as "export" delays) (Fig. 1*A* and *Materials and Methods*). Delays were measured by comparing onset times as determined by regression analysis (Fig. 1*B* and *Materials and Methods*).

To estimate elongation kinetics, we compare the onset times of introns 1 and 7, which lie 6.3 kb apart on the primary *Lfng* transcript (Fig. 1*A* and *Materials and Methods*). There was no significant time delay in these introns' expression (intron 1: 10.2 ± 2.6 min, intron 7: 9.4 ± 2.3 min; Fig. 1 *C*, *i*; $P > 0.7$), indicating that elongation is indeed very rapid. The extended lag before detecting induced transcripts is probably caused by delays in hormone transport and transcript initiation. Recently reported elongation rates of 3.5–4 kb/min (24) predict an elongation time of 1.5–1.7 min for *Lfng*, which is too fast for us to measure. We would also not expect to be able to measure the elongation kinetics of the even shorter *Hes7* gene (Fig. 1 *D*, *i*).

Such short elongation delays would not contribute greatly to transcript kinetics, and so we tested if RNA splicing might impose a significant delay. We measured the splicing kinetics of *Lfng* and *Hes7* using primer pairs selective for unprocessed and processed transcripts. We find that splicing is much slower than elongation. For *Lfng* introns 1 and 7, the mean delay between spliced and unspliced transcript accumulation is 7.9 ± 2.3 min and 7.4 ± 3.6 min, respectively (Fig. 1 *C*, *ii* and *iii* and *E*; Table 1; and *Materials and Methods*). *Hes7* introns 1 and 3 splice more slowly (two-way ANOVA, $P = 0.05$) with delays of 11.6 ± 3.2 and 11.7 ± 2.4 min, respectively (Fig. 1 *D*, *ii* and *iii* and *E*). These timings are broadly consistent with previous measurements of ex vivo splicing kinetics in cultured cells (24).

mRNA synthesis depends also on postsplicing mRNA maturation and nuclear export into the cytoplasm. The former has been reported to be rapid and cotranscriptional (32, 33). This is indeed the case for polyadenylation in our inducible system; we were unable to detect a delay between the splicing of *Hes7* exons 1/2 and polyadenylation of the transcripts (Fig. 1*F*).

By contrast, export from the nucleus appears even slower than splicing. We analyzed the appearance of spliced RNAs in the nucleus and cytoplasm, and found similar mean delays between splicing across *Lfng* exons 1/2 and 7/8 and the arrival of transcripts in the cytoplasm (16.6 ± 2.1 and 17.6 ± 2.3 min, respectively) (Fig. 1 *C*, *ii* and *iii* and *E*). The similarity of these measurements indicates that elongation is indeed rapid and that there is little delay between the splicing of these *Lfng* exons. *Hes7* export is yet slower, at 25.4 ± 2.4 and 21.0 ± 3.9 min for spliced exons 1/2 and 3/4, respectively ($P < 0.01$; Fig. 1 *D*, *ii* and *iii* and *E*), confirming that nuclear export ex vivo delays production of functional for *Lfng* and *Hes7* mRNAs even more than splicing.

Transcript Elongation Is Rapid in Vivo. To measure transcript kinetics in vivo, we analyzed *Lfng* and *Hes7* expression during embryonic segmentation. As PSM cells mature and become displaced during axial extension, the segmentation clock slows, causing anterior cells to activate transcription of cycling genes slightly later than posterior cells. This lag between generating a primary transcript and its export into the cytoplasm means that although nuclear and cytoplasmic cycling transcripts show very similar expression patterns (10, 34), the domain of nuclear transcripts lies slightly anterior to that of cytoplasmic transcripts (9) (Fig. 2 *A*, *iv* and *v*). Thus, time delays correspond to spatial displacements (9).

We used FISH to define the anterior boundaries of progressive stages of mRNA synthesis, maturation, and localization in mouse embryonic day (E) 10.5 embryos (Fig. 2*A*). For each transcript species, we plotted anteroposterior intensity distributions and defined the anterior boundary as the anterior inflection point because it could be identified reliably, and because simulations showed it to be relatively invariant to probe-specific differential sensitivity. Nuclei were stained to allow computational separation of nuclear and cytoplasmic signals. Spatial displacements were converted into temporal delays based on the mathematical relationship between position in the PSM, distance between successive transcript stripes in the PSM, and clock period (*Materials and Methods*) (9).

To assay elongation kinetics, we used double-label FISH to compare the expression domains of *Lfng* introns 1 and 7. Both probes stain only dots in the nucleus, as expected for detection of nascent, primary transcripts and consistent with splicing being complete before transcripts are released from chromatin. We were unable to visualize a displacement between these probes' anterior boundaries ($n = 4$; Fig. S1), indicating that transcriptional elongation in vivo is rapid, like in cultured cells.

Measuring in Vivo Splicing Kinetics. A comparison between intron-encoding and intronless *luciferase-Hes7* reporters in the mouse PSM previously indicated that intron-splicing retards expression of the *Hes7* segmentation gene by about 19 min (31). Such a delay would contribute substantially to the segmentation clock but is considerably longer than the 5- to 10-min delay typical of cultured cells (24, 35).

We determined the kinetics of *Lfng* and *Hes7* splicing in the mouse PSM directly using double-labeled FISH. We visualized unspliced RNA with probes against the first *Lfng* or *Hes7* introns and detected spliced transcripts with probes spanning exons 1–4

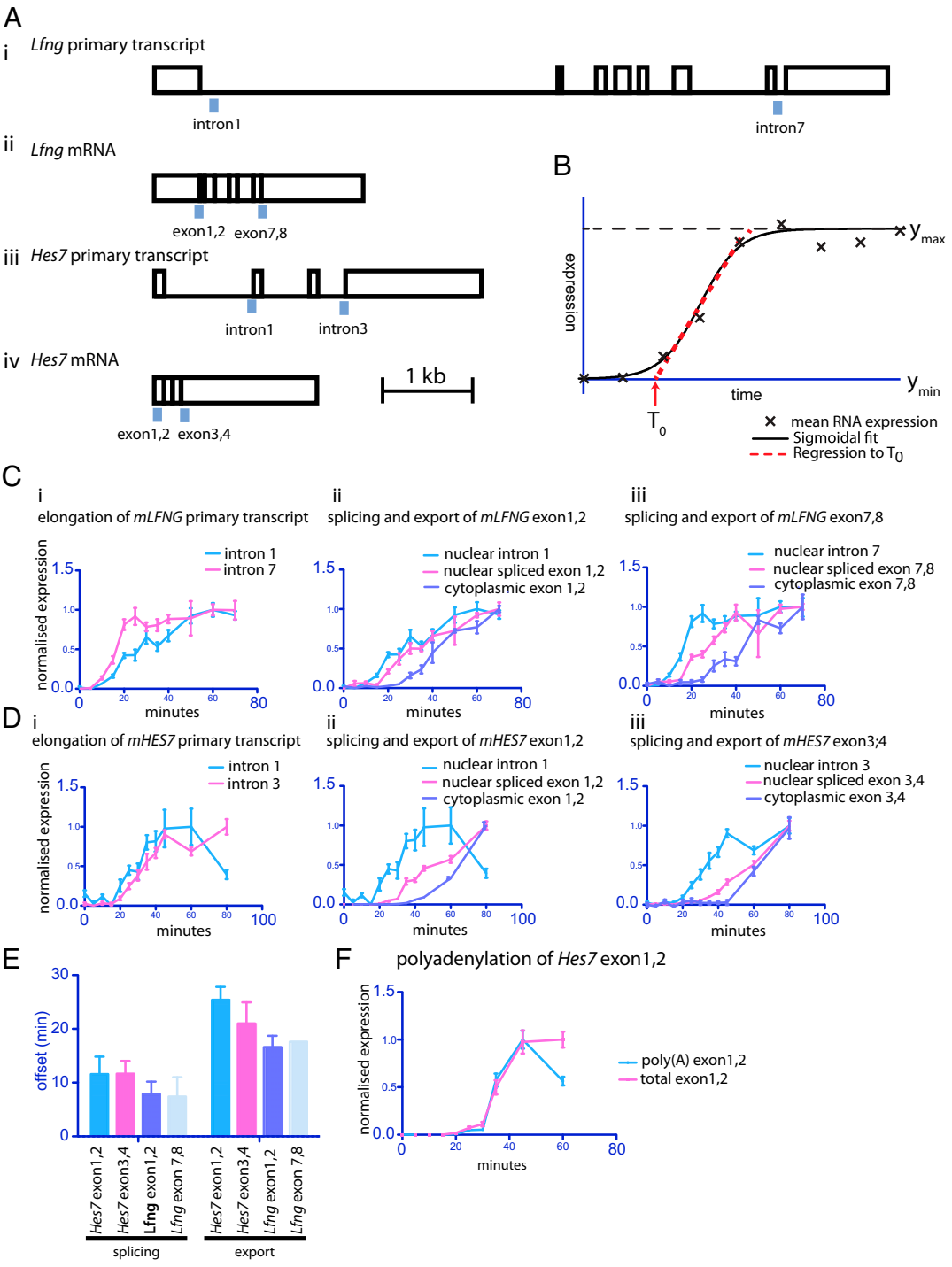

Fig. 1. Ex vivo measurement of transcript elongation, splicing, and export delays of mouse *Lfng* and *Hes7*. (*A*) Schematic indicates the position of qRT-PCR target amplicons on *Lfng* pre-mRNA (*i*), *Lfng* mRNA (*ii*), *Hes7* pre-mRNA (*iii*), and *Hes7* mRNA (*iv*). (*B*) Graph illustrates RNA accumulation kinetics fitted to a sigmoidal curve (*Materials and Methods*). The red dashed line indicates how regression from the inflection point to the baseline expression level gives a proxy measure for expression onset (T_0). Timings generated by this method are relatively insensitive to differences in expression levels and amplification efficiencies (with the latter being exemplified by *Lfng* introns 1 and 7). Graphs illustrate accumulation of the indicated species of mouse *Lfng* (*C*) or *Hes7* (*D*) transcript measured by qRT-PCR after induction of expression. Representative examples from three biological replicates are shown. Error bars indicate SD from three technical replicates (also in *E* and *F*). (*E*) Chart shows delay between the onset of accumulation of pre-mRNA and spliced mRNA (splicing offset) and nuclear mRNA and cytoplasmic mRNA (export offset). (*F*) Accumulation of polyadenylated *Hes7* exon 1,2 vs. total *Hes7* exon 1,2.

of *Lfng* or *Hes7*, which have only short contiguous homologies to unspliced products. Evidence that such bridging probes fail to detect unspliced products comes from their detection of posteriorly displaced domains compared with intron probes (e.g., Fig. 2*A*) and the failure of short contiguous probes to detect any transcripts under our conditions.

Both probes show typical patterns of cyclic *Lfng* staining in the PSM. Signal from unspliced probes is only nuclear, whereas

Table 1. Ex vivo and in vivo delay measurements

Gene	Region	Ex vivo splicing delay	Ex vivo export delay	In vivo splicing delay	In vivo export delay
Mouse *Lfng*	Intron 1	7.9 ± 2.3 (3)	16.6 ± 2.1 (3)	9.7 ± 2.8 (5)	16.1 ± 5.7 (13)
	Intron 7	7.4 ± 3.6 (3)	17.6 ± 2.3 (3)		
Mouse *Hes7*	Intron 1	11.6 ± 3.2 (3)	25.4 ± 2.4 (3)	12.5 ± 6.3 (8)	17.0 ± 8.3 (8)
	Intron 3	11.7 ± 2.4 (3)	21.0 ± 3.9 (3)		
Chick *Lfng*				6.7 ± 3.7 (22)	9.2 ± 4.8 (21)
Chick *Her1*				5.5 ± 2.2 (7)	9.6 ± 2.7 (11)
Chick *Nrarp*					11.0 ± 4.5 (11)
Zebrafish *Her1*				2.4 ± 1.1 (8)	3.36 ± 1.0 (8)

Values are in minutes, errors are SDs, and *n* values are indicated in parentheses.

splice-specific probes stain both nucleus and cytoplasm, as previously observed with longer individual probes targeted to *Lfng* and *Hes7* (11, 12, 34) (Figs. 2 *B* and 3 *A*, iii). The domains of unspliced and nuclear spliced transcripts largely overlap, but the anterior boundary of the former lies consistently anterior of the latter, with a spatial displacement corresponding to a splicing

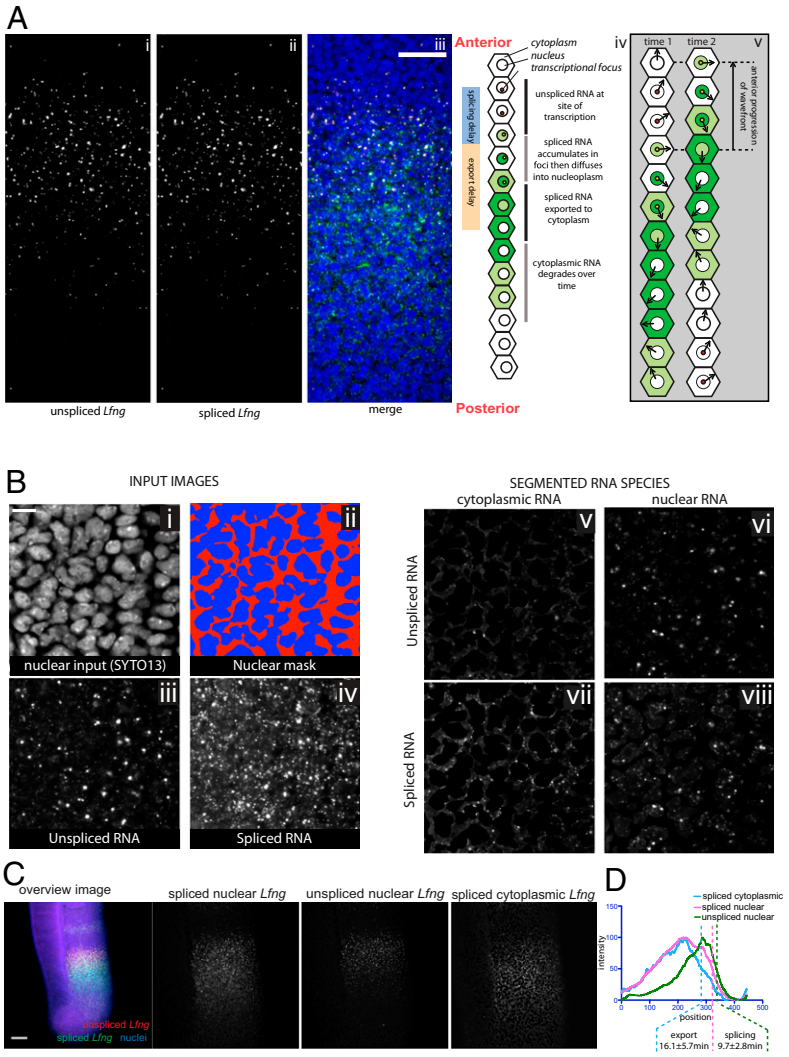

Fig. 2. In vivo *Lfng* transcript delays measured by multilabeled FISH. (*A*) FISH detection of unspliced *Lfng* (*i*) and spliced *Lfng* (*ii*) in E10.5 mouse PSM, with merge (*iii*). Nuclei are stained using SYTO13. In this and subsequent figures, anterior is upward. (Scale bar, 500 μm.) (*iv*) Due to slowing of the clock as cells mature, anterior cells are in an earlier phase (as shown by arrow direction in *v*) of the gene expression cycle than posterior cells. (*v*) Local synchrony leads to kinematic anterior progression of the expression domain. Red and yellow nuclear dots show sites of nascent unspliced and spliced nuclear transcripts, and shades of green represent levels of spliced transcript. (*B*) Segmentation of multicolor FISH images. The nuclear channel (*i*) was manually thresholded to a binary image (red and blue) (*ii*), and used with stacked images of unspliced (*iii*) and spliced (*iv*) RNA to generate images of the unspliced cytoplasmic (*v*), unspliced nuclear (*vi*), spliced cytoplasmic (*vii*), and spliced nuclear (*viii*) signals. Scale bar: 10 mm. (*C*) Z-average projections of multicolor *Lfng* FISH z-stacks generated after segmentation. (Scale bar: 100 μm unless otherwise defined.) (*D*) *Lfng* signal intensity plots of images in *C* measured from the posterior to anterior of the expression domain and averaged across the width of the PSM. The anterior inflection points of the various expression domains used to measure the mean splicing and export offset times are marked with vertical dashed lines show (also in subsequent graphs).

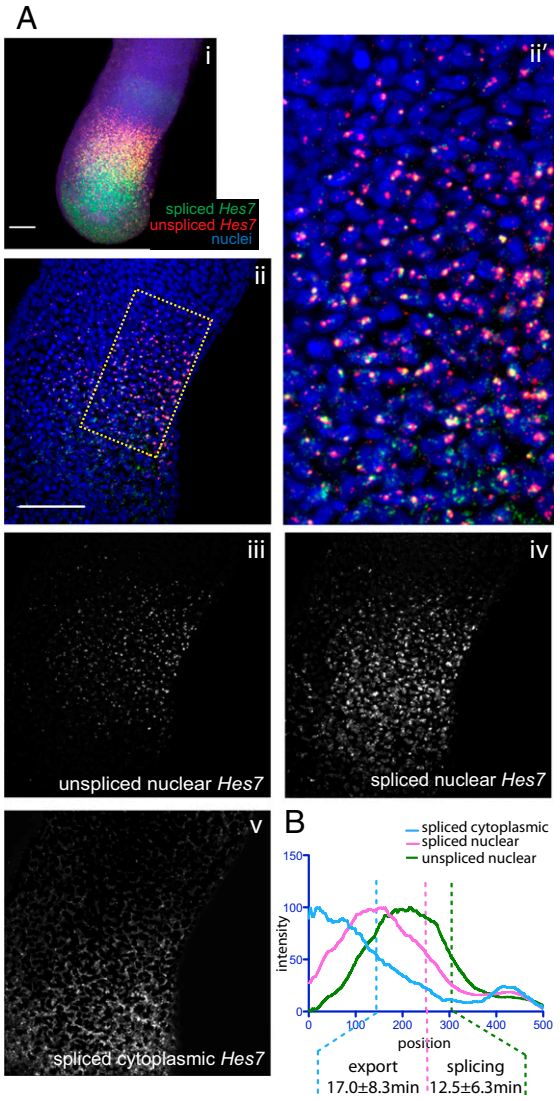

Fig. 3. Estimation of transcript export and splicing delays of *Hes7* in the mouse PSM. (*A*, *i*) Maximum z-projection of FISH against Mouse *Hes7*. Segmentation of higher magnification FISH images was conducted as in Fig. 2*B*. An example source image (*ii*) and detailed view of the source image indicated by the hatched area (*ii′*) are shown, along with the segmented images representing unspliced nuclear pre-mRNA (*iii*), spliced nuclear mRNA (*iv*), and spliced cytoplasmic mRNA (*v*). Average z-projections are shown. (Scale bar: 100 μm.) (*B*) Intensity plots of images in *A*, *iii–v* measured from the posterior to anterior of the expression domain, averaged across the width of the PSM.

delay of 9.7 ± 2.8 min for *Lfng* (Figs. 2 *C* and *D* and *Materials and Methods*). *Hes7* also suffers a transcriptional delay associated with splicing (12.5 ± 6.3 min; Fig. 3*B*), which is of similar magnitude to that for *Lfng*. Together, our results indicate that splicing retards the in vivo production of mature mRNA substantially more than transcriptional elongation.

Transcript Export Contributes Substantially to Transcriptional Latency. In cultured cells, mRNA export is even slower than splicing. To test if this also holds in vivo, we used splice-specific probes to compare the appearance of spliced mRNA in the nucleus and the cytoplasm. For *Lfng*, we find an export delay of 16.1 ± 5.7 min (Fig. 2*D*), consistent with that measured in cultured cells. For *Hes7*, the delay in vivo is 17.0 ± 8.3 min (Fig. 3*B*), which is not significantly different from that for *Lfng* (unlike in cultured cells; Fig. 1*E* and Table 1). These data suggest that export delays are likely to contribute even more to clock period than splicing delays.

Export of transcripts into the cytoplasm is functionally linked to splicing; the transcription/export complex is deposited during splicing at exon junctions and interacts with the nuclear export receptor Tap/Nuclear RNA export factor 1 (36, 37). To test if lack of introns affects in vivo export kinetics, we examined the *Notch-regulated-ankyrin-repeat-protein* (*Nrarp*) intronless transcript, which also cycles in the PSM (38).

In accord with previous reports, we detect a strong, dynamic *Nrarp* signal (Fig. 4 *A*, *i*) that accumulates in a relatively broad region due to increased transcript stability (38). The latter should not affect our determination of delay times, because onset (anterior) boundaries are unaffected by increased transcript persistence. Comparing the domains of cytoplasmic and nuclear *Nrarp* transcripts yields a delay of 14.5 ± 4.9 min (Figs. 4 *A*, *ii–iv* and *B*), similar to those of the intron-containing transcripts. Thus, the

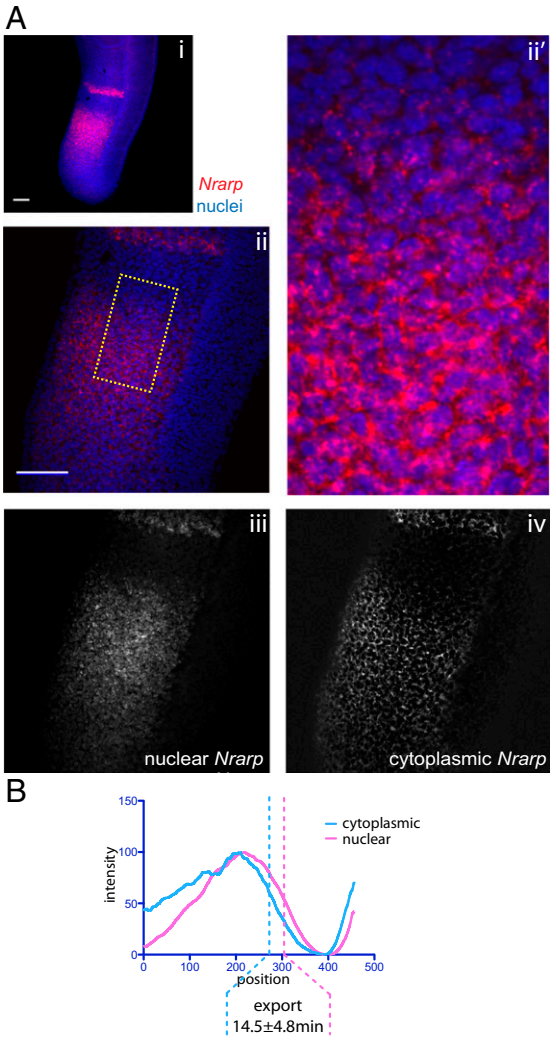

Fig. 4. Estimation of transcript export delays of *Nrarp* in the mouse PSM. (*A*, *i*) Maximum z-projection of FISH against Mouse *Nrarp*. Segmentation of higher magnification FISH images was conducted as in Fig. 2*B*. An example source image (*ii*) and detailed view of the source image indicated by the hatched area (*ii′*) are shown, along with the segmented images representing unspliced nuclear pre-mRNA (*iii*), spliced nuclear mRNA (*iv*), and spliced cytoplasmic mRNA (*v*). Average z-projections are shown. (*B*) Intensity plots of images in *A*, *iii–v* measured from the posterior to anterior of the expression domain, averaged across the width of the PSM.

lack of introns in *Nrarp* does not in itself impair or assist mRNA export.

Interspecies Differences in Transcription Kinetics. The segmentation clock period varies widely between species, consistent with their differing developmental paces. For example, the segmentation clock oscillates about threefold more slowly in humans than in mice (39, 40). To study species-specific differences in more detail, we analyzed splicing and export delays in chicken embryos, whose segmentation clock is about 30 min shorter than in mice.

The pattern of oscillatory gene expression in the chick PSM resembles that in the mouse (41, 42), and 13–18 somite chicken embryos and mouse E10.5 embryos show similar distributions of nuclear dots and diffuse cytoplasmic signal for unspliced and spliced *Lfng* (Fig. 5 *A*, *ii–v*). The displacement between these signals predicts a splicing offset of 6.7 ± 3.7 min in the chick, 3 min shorter than the splicing delay in the mouse ($P = 0.07$; Fig. 5 *A*, *vi* and Table 1). Equivalent experiments on chick *Her1*/*hairy1* reveal splicing delays of 5.5 ± 2.2 min (Fig. 5*B* and Table 1), which is, again, less than in the mouse.

For the nuclear export of chick *Lfng* and *Her1*/*hairy1* transcripts, we find offsets of 9.2 ± 2.7 min and 9.6 ± 2.7 min, respectively, which is about 7 min shorter than the delays in the mouse (Fig. 5 *A* and *B* and Table 1). The export delay of chick *Nrarp* is also shorter than in the mouse (11.0 ± 4.5 min; Fig. 5*C* and Table 1). Thus, splicing and export in the chick PSM are significantly faster than in the mouse, in accord with the former's more rapid segmentation clock.

We also measured splicing and export kinetics in the zebrafish, with its much faster, 30-min segmentation clock cycle. For *her1*, we find splicing and export delays of 2.4 ± 1.1 min and 3.4 ± 1.0 min, respectively (Fig. 6), consistent with the previous estimates of transcriptional delays in fish (9).

Discussion

Splicing Is Slow Compared with Transcriptional Elongation. We have measured the in vivo kinetics of mRNA production to assess likely contributions of transcriptional delays toward the vertebrate segmentation oscillator. We show that in both cultured cells and the PSM, elongation of *Lfng* and *Hes7* segmentation transcripts is much faster than their splicing, which, in turn, is faster than their export. We also find longer in vivo transcriptional delays (especially those associated with export) for species with slower segmentation clocks.

Transcriptional elongation of our relatively short genes in mouse cells and embryos was too rapid for us to measure, consistent with previous fast rates measured ex vivo (Fig. S1) and also with a recent measurement of transcriptional elongation during zebrafish segmentation (4.8 kb/min) (22, 24–26, 43). Such rapidity may partly explain why segmentation is normal in mice with a lengthened *Lfng* gene (44).

Both ex vivo and in chick and mouse embryos, RNA splicing of these transcripts introduces an 8- to 12-min delay (Figs. 1 and

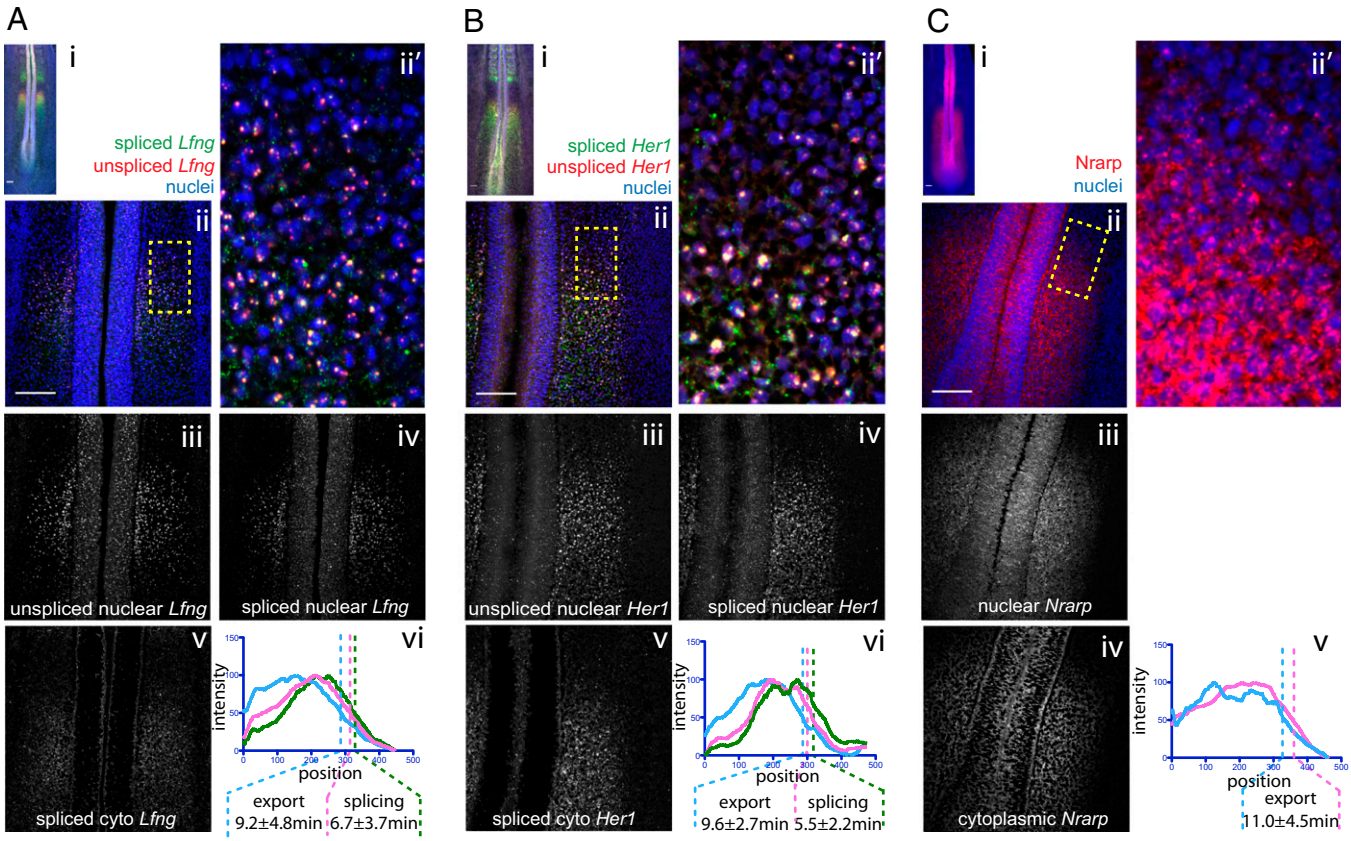

Fig. 5. mRNA export and splicing delays measured in the chick PSM. Maximum z-projection of FISH for chick *Lfng* (*A*), *Hairy1*/*Her1* (*B*), and *Nrarp* (*C*) shows (*i*) embryo posteriors. Higher magnification images (*ii*) were segmented as in Fig. 2*B* to generate images of unspliced nuclear RNA (*iii*), spliced nuclear RNA (*iv*), and spliced cytoplasmic RNA (*v*). Anteroposterior intensity profile graphs of one PSM are shown for each RNA species. Anterior inflection points are shown, along with average export and splicing offsets from Table 1. Maximum z-projection of FISH against chick *Lfng* (*A*), *Hairy1*/*Her1* (*B*), and *Nrarp* (*C*) shows representative embryos at low (*i*) and higher (*ii* and *ii′*) magnification. Sets *iii–v* are as labeled, except that *A*, *vi*; *B*, *vi*; and *C*, *v* show the intensity graphs from which measurements were drawn.

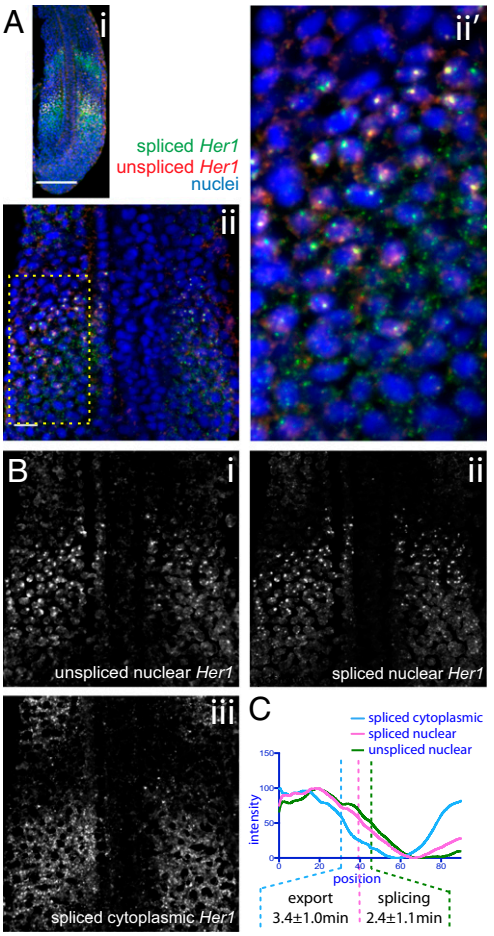

Fig. 6. Estimation of mRNA export and splicing delays in the zebrafish PSM. (*A*) Maximum z-projection of FISH against zebrafish *Her1*. (*B*) Segmentation of higher magnification FISH against Her1 shows the source image (*i*), unspliced nuclear pre-mRNA (*ii*), spliced nuclear mRNA (*iii*), and spliced cytoplasmic mRNA (*iv*). (*C*) Intensity plots of images in *B* measured from the posterior to anterior of the expression domain, averaged across the width of the PSM, and corrected for skew (*Materials and Methods*). Anterior inflection points of the posterior expression domain are indicated with dashed lines for each RNA species.

4 and Table 1). Nevertheless, all or most processing seems to occur cotranscriptionally (i.e., while transcripts are still attached to chromatin). Accordingly, we detect intron signals only as dots, presumably representing the sites of transcription (22, 34), and not in the nucleoplasm as with splice-specific probes (e.g., Fig. 2 *A*, *i* and *ii*).

Different introns show similar although not identical ex vivo kinetics (24). Because elongation is so rapid, the offset between splicing tandem introns will be minimal, implying that splicing delays should be largely independent of the number of introns and depend on that of the slowest or last intron. Consistent with this view, the delays between synthesis of the first and last introns of *Lfng* and *Hes7* and export of spliced mRNA are essentially the same (Table 1), despite the former requiring excision of several extra introns before export commences. Concurrent splicing of multiple introns is also in agreement with a recent report that removing *Hes7* introns 1 and 3 in transgenic mice reduced expression kinetics by only 5 min (45). If splicing were sequential, one would expect a reduction of 10–20 min (24, 46).

Nuclear Export Provides a Major Postsplicing Transcriptional Delay. Nuclear export does not proceed until splicing is complete (47); therefore, its delay should supplement that of splicing. We did not detect a delay between the appearance of total and polyadenylated spliced RNA (Fig. 1*F*), supporting the view that cleavage and polyadenylation are rapid and occur very soon after completion of the last exon (33).

Export delays are significant in all the systems we analyzed, being equal to those of splicing in zebrafish and even longer in mouse and chicken embryos (Table 1). Together, the two delays explain most of the total transcript delay determined during zebrafish segmentation (9).

A likely source of export delay is the requirement for mature mRNA to move from the site of transcription to the nuclear periphery. For freely diffusing transcripts, such a step would be extremely rapid. However, our much slower measurements are consistent with previous (albeit divergent) estimates, which suggest that transcripts undergo restricted diffusion at rates that vary according to their messenger RNP composition (48–50). Additional export delays could also arise during docking of transcripts with the pores, and transcript translocation across the pore into the cytoplasm. Another potentially slow postsplicing step is detachment from chromatin, which has been reported to be slow in mouse bone marrow-derived macrophages for some long, processed transcripts (43). We are unable to time this step for our genes in vivo.

Postsplicing Events Dominate Transcriptional Delays During Segmentation. Our measurements indicate that splicing and export delays together correspond to 16–25% of the segmentation clock period in the three species examined. The period of a delayed negative-feedback oscillator is about twice the sum of its delays, so that our measured transcriptional delays alone account for about half of the total clock period (8). *Hes7* transcripts and proteins have ex vivo half-lives of about 20 min (10, 51). These degradation kinetics will contribute to the delays in the clock circuitry, and thereby explain much of the rest of its period. Thus, a single component transcriptional circuit can explain the observed oscillations, at least for the zebrafish, chick, and mouse.

Previous work has suggested that the *Hes7* splicing delay is a major contributor to the mouse segmentation clock. Accumulation of *Hes7* transcripts and Hes7 protein in the PSM appears substantially out of phase (10), with an estimated delay of 33 min (31). This result is broadly consistent with our measurements of the delay between initiating *Hes7* transcription and accumulation of cytoplasmic *Hes7* mRNA (29.5 min; Figs. 1*E* and 3*B*).

Our measurements suggest that postsplicing delays contribute more to clock period than splicing. Takashima and colleagues (31) found that the presence of the *Hes7* introns in a *luciferase* reporter gene delay the appearance of luciferase activity by 19 min, which they attributed to the time required to remove introns. We find much more rapid splicing of endogenous *Hes7* (12.5 min ex vivo and 11.6 min in vivo) and of chick *hairy1*/*Her1* and mouse and chick *Lfng* (Table 1).

Also, intron-free *luciferase-Hes7* transcripts seem to be exported much more rapidly than the transcripts we tested, including naturally intronless *Nrarp* transcripts. Thus, active luciferase protein becomes detectable 10 min after the onset of transcription (31) which, if transcriptional elongation and protein translation and folding takes 2–4 min, would correspond to an export delay of 6–8 min. *Nrarp* suffers a much longer delay of 14.5 ± 4.9 min (Table 1), which is similar to that of endogenous *Hes7* and *Lfng*.

Possible explanations for these apparent discrepancies include differences between the transcript kinetics of endogenous *Hes7* and the artificial *luciferase* fusion genes, and different behaviors of transcripts that are naturally intron-free and those derived by intron removal (52). Thus, the two classes of transcript may be packaged into RNPs containing different RNA-binding proteins, which would influence the kinetics of mRNA diffusion in the nucleus and perhaps of docking and translocation into the cytoplasm (49).

Interspecies Changes in RNA Maturation Kinetics Are Coordinated with Clock Period. Because nuclear export seems to be the predominant transcriptional delay in generating a functional mRNA, it should be a major contributor to setting the pace of the segmentation clock. Export offsets between mouse, chick, and zebrafish embryos indeed vary with the native clock period, and the delays, at least for mouse and chick, do not appear to vary significantly between genes.

Export delay accounts for a consistent proportion of the mouse, chick, and zebrafish somite clock periods (12.3 ± 1.8%), as do splicing delays in the chick and mouse (8.3 ± 1.6%). Thus, the clock period of a given species is linked to its kinetics of gene expression, presumably because both are integrated with the pace of development. This is in contrast to the more complex circadian oscillator, whose circuitry is designed to be invariant to a wide variety of developmental and environmental perturbations (53).

Nevertheless, differences in the kinetics of transcript production do not explain all aspects of the clock circuit. The human somite clock has a period of about 6 h, and *Hes1* transcription oscillates with a similar period in human cell culture (40). This is much slower than that of the chick and mouse, yet the overall kinetics of transcript production do not differ much between human and mouse cells in culture, and the human *Lfng* and *hairy/Hes* genes have similar lengths to their mouse and chick counterparts (21, 22, 24, 46). The divergence in clock period must therefore derive from other sources.

It is formally possible that the three- to fourfold slower somite clock period in humans is due to exceptionally slow, tissue-specific kinetics of gene expression in the PSM. However, more likely, the long period is substantially due to increased half-lives of human segmentation proteins and RNAs, and perhaps slower activation and compartmentalization of autorepressive gene products (51). Future experiments will establish a more detailed understanding of in vivo transcript kinetics and how individual steps of synthesis and maturation contribute to defining different segmentation clock periods.

Materials and Methods

Constructs and Culture. *pGENE_LFNG* and *pGENE_HES7* were constructed by insertion of genomic mouse *Lfng* or *Hes7* and 1 kb of downstream sequence into the SacII and AgeI restriction site of *pGENE* (Invitrogen) by means of recombination-driven cloning (54).

C3H10T1/2 cells were stably transfected in a stepwise fashion with *pSWITCH* and *pGENE_LFNG* or *pGENE_HES7* and grown in DMEM plus 10% FBS (vol/vol), penicillin (100 U/mL), streptomycin (100 μg/mL), hygromycin B (100 μg/mL), and zeocin (250 μg/mL). Transcription was induced with 10 nM mifepristone (Sigma).

WT *C57BL/6J* mice were used for all murine experiments. Embryos were collected from pregnant females and fixed as above. White Leghorn chicken embryos (Henry Stuart) were grown at 37 °C to Hamburger Hamilton stage 13–14 before isolation from extraembryonic membranes and fixation overnight in 4% phosphate buffered formaldehyde at 4 °C. Fixed embryos were dehydrated in methanol for storage at −20 °C before FISH. WT zebrafish embryos were grown at 28 °C, fixed at the ∼10-somite stage as above, dechlorinated, and removed from their yolks after rehydration.

Experiments were conducted in strict adherence to the Animals (Scientific Procedures) Act of 1986 and UK Home Office Codes of Practice for use of animals in scientific procedures.

In Situ Hybridization. FISH probes were generated by in vitro transcription of T3 promoter-containing PCR products generated from genomic DNA or RT-PCR of total RNA. Primers are listed in Table S1. Hybridization and detection were carried out as described previously (55). Probes were detected using 1:1,000 peroxidase-conjugated anti-digoxigenin (DIG) Fab (Roche) or 1:100 peroxidase-conjugated antibody (PerkinElmer), and were developed using Tyramide Signal Amplification (TSA)-cyanine 5 (Cy5) or TSA-Cy3 reagents (PerkinElmer) for unspliced pre-mRNA and spliced mRNA, respectively. For dual-probe FISH, probes were cohybridized and fluorescein was detected first as in single-color FISH. Peroxidase activity was quenched by treatment in 2% H_2O_2 in methanol (vol/vol) for 30 min. After rehydration in maleic acid buffer, embryos were blocked and DIG was detected as in the single-color fluorescent in-situ protocol. Nuclei were stained using SYTO13 (Invitrogen) at a 1:1,000 dilution in PBS for at least 2 h.

RNA Isolation and Assays. Cells were cooled in a shallow ice bath, washed in ice-cold PBS, and collected by gentle scraping. Nuclear and cytoplasmic portions of the cells were fractionated by centrifugation before column-based purification of RNA (QIAGEN) and DNase treatment using Turbo DNase (Ambion).

Transcript levels were assayed from 100 ng of RNA using the one-step MESA green qRT-PCR kit (Eurogentec) and the primers listed in Table S2. Expression levels were calculated using the standard methods and normalized to coassayed levels of *Gapdh* transcripts. To determine the induction point of an RNA species (t_0), curves were fit to $y = y_{min} + (y_{max} - y_{min})/(1 + 10^{((K - x)\cdot 2/((K - t_0)\cdot \ln(10)))})$ using Prism 5.0 (GraphPad; supplemental methods for curve fitting and normalization are provided in *Curve Fitting*). Cytoplasmic unspliced RNA failed to amplify, consistent with successful fractionation of RNA.

Image Capture and Analysis. Embryos were mounted on glass slides, and images were captured using a Zeiss LSM700 microscope. The geometry of embryos used for FISH analysis was determined from 19-μm confocal optical sections of embryos captured using a C-apochromat 10×/0.45-W lens with a 0.5× digital zoom. For image segmentation, embryos were reimaged using a Plan-Neofluar 25×/0.8-Imm Korr DIC lens with a 0.5× digital zoom to generate ten 2.0-μm sections. In each z-section, pixels were classified as nuclear or nonnuclear (cytoplasmic) based on a manually determined threshold of the nuclear signal. An image multiplication function was then used to derive two images from each channel of FISH staining, one corresponding to the nuclear FISH signal and the other nonnuclear (cytoplasmic). Z-stacks were average-projected, and signal intensity was measured using the "plot profile" function in ImageJ (National Institutes of Health) along the anteroposterior axis PSM averaged across the entire width. Plots for each FISH were subjected to a 10-point locally weighted scatterplot smoothing algorithm using Prism 5.0 software (GraphPad), and the anterior inflection point of the expression domain was recorded for each segmented image.

The spatial interval between inflection points was converted into a temporal offset as described previously (full derivation is provided in ref. 9). In summary, stained embryos were used to generate a curve relating local frequency (and hence period) to axial position, using interstripe distances and the known maximum cycling frequency (e.g., 0.5 cycles per hour in the mouse). The data were fitted to the following equation relating local and maximal frequencies [$\omega(x)$ and ω_0 respectively], and to axial position [$\mu(x)$], somite length [S_0] and the measured wavelength between two waves of gene expression bounding $\mu(x)$ [$S(x)$]:

$$\text{Relative oscillation frequency} = \frac{\omega(x)}{\omega_0} = 1 - \frac{\mu(x) S_0}{S(x)}.$$

Temporal offsets were calculated from the spatial offset (a) and periodicity of somite production (p) visualized by in situ hybridization by means of the following equation:

$$\text{Temporal offset} = \frac{a\, p\, \omega_0}{S(x)\omega(x)}.$$

Because this method of analysis requires two domains of gene expression in each PSM, we could only measure delays in embryos with an anterior, nonoscillating expression stripe (so-called "pattern phase I and II embryos") (3). In general, we found no significant correlation between the axial position of the oscillating stripe (which relates to patterning phase) and the calculated delay in our FISH datasets (Spearman correlation, $P > 0.05$), except for mouse *Nrarp* export ($P = 0.02$) (but not splicing) and chick *Lfng* splicing ($P = 0.04$) [but not export (Fig. S2)]. Thus, our calculations of local oscillation frequency correct effectively for the slowing of the clock as cells approach the anterior determination front.

ACKNOWLEDGMENTS. We thank Anya Hanisch, Maxine Holder, and Cristian Soza-Ried for advice on zebrafish experimentation and husbandry, and Gavin Kelly for his help devising the qRT-PCR curve-fitting equation. We also thank David Bentley, Rippei Hayashi, Cristian Sosa-Ried, and Jesper Svejstrup for comments on the manuscript. We are particularly grateful to Julian Lewis, whose previous work inspired our approach, for advice and invaluable mentorship of N.P.H. in mathematical techniques required for the project. This work was supported by Cancer Research UK.

1. Cooke J, Zeeman EC (1976) A clock and wavefront model for control of the number of repeated structures during animal morphogenesis. *J Theor Biol* 58(2):455–476.
2. Oates AC, Morelli LG, Ares S (2012) Patterning embryos with oscillations: Structure, function and dynamics of the vertebrate segmentation clock. *Development* 139(4):625–639.
3. Palmeirim I, Henrique D, Ish-Horowicz D, Pourquié O (1997) Avian *hairy* gene expression identifies a molecular clock linked to vertebrate segmentation and somitogenesis. *Cell* 91(5):639–648.
4. Pourquié O (2011) Vertebrate segmentation: From cyclic gene networks to scoliosis. *Cell* 145(5):650–663.
5. Jiang YJ, et al. (2000) Notch signalling and the synchronization of the somite segmentation clock. *Nature* 408(6811):475–479.
6. Masamizu Y, et al. (2006) Real-time imaging of the somite segmentation clock: Revelation of unstable oscillators in the individual presomitic mesoderm cells. *Proc Natl Acad Sci USA* 103(5):1313–1318.
7. Delaune EA, François P, Shih NP, Amacher SL (2012) Single-cell-resolution imaging of the impact of Notch signaling and mitosis on segmentation clock dynamics. *Dev Cell* 23(5):995–1005.
8. Lewis J (2003) Autoinhibition with transcriptional delay: A simple mechanism for the zebrafish somitogenesis oscillator. *Curr Biol* 13(16):1398–1408.
9. Giudicelli F, Özbudak EM, Wright GJ, Lewis J (2007) Setting the tempo in development: An investigation of the zebrafish somite clock mechanism. *PLoS Biol* 5(6): e150.
10. Bessho Y, Hirata H, Masamizu Y, Kageyama R (2003) Periodic repression by the bHLH factor Hes7 is an essential mechanism for the somite segmentation clock. *Genes Dev* 17(12):1451–1456.
11. Morimoto M, Takahashi Y, Endo M, Saga Y (2005) The Mesp2 transcription factor establishes segmental borders by suppressing Notch activity. *Nature* 435(7040): 354–359.
12. Saga Y, Hata N, Koseki H, Taketo MM (1997) *Mesp2*: A novel mouse gene expressed in the presegmented mesoderm and essential for segmentation initiation. *Genes Dev* 11(14):1827–1839.
13. Chen J, Kang L, Zhang N (2005) Negative feedback loop formed by Lunatic fringe and Hes7 controls their oscillatory expression during somitogenesis. *Genesis* 43(4):196–204.
14. Dale JK, et al. (2003) Periodic notch inhibition by lunatic fringe underlies the chick segmentation clock. *Nature* 421(6920):275–278.
15. Ferjentsik Z, et al. (2009) Notch is a critical component of the mouse somitogenesis oscillator and is essential for the formation of the somites. *PLoS Genet* 5(9):e1000662.
16. Krol AJ, et al. (2011) Evolutionary plasticity of segmentation clock networks. *Development* 138(13):2783–2792.
17. Oates AC, Gorfinkiel N, González-Gaitán M, Heisenberg C-P (2009) Quantitative approaches in developmental biology. *Nat Rev Genet* 10(8):517–530.
18. Ingolia NT, Lareau LF, Weissman JS (2011) Ribosome profiling of mouse embryonic stem cells reveals the complexity and dynamics of mammalian proteomes. *Cell* 147(4): 789–802.
19. Siwiak M, Zielenkiewicz P (2010) A comprehensive, quantitative, and genome-wide model of translation. *PLOS Comput Biol* 6(7):e1000865.
20. Swinburne IA, Silver PA (2008) Intron delays and transcriptional timing during development. *Dev Cell* 14(3):324–330.
21. Ben-Ari Y, et al. (2010) The life of an mRNA in space and time. *J Cell Sci* 123(Pt 10): 1761–1774.
22. Darzacq X, et al. (2007) In vivo dynamics of RNA polymerase II transcription. *Nat Struct Mol Biol* 14(9):796–806.
23. Lionnet T, et al. (2011) A transgenic mouse for in vivo detection of endogenous labeled mRNA. *Nat Methods* 8(2):165–170.
24. Singh J, Padgett RA (2009) Rates of in situ transcription and splicing in large human genes. *Nat Struct Mol Biol* 16(11):1128–1133.
25. Wada Y, et al. (2009) A wave of nascent transcription on activated human genes. *Proc Natl Acad Sci USA* 106(43):18357–18361.
26. Hanisch A, et al. (2013) The elongation rate of RNA polymerase II in zebrafish and its significance in the somite segmentation clock. *Development* 140(2):444–453.
27. Mor A, Shav-Tal Y (2010) Dynamics and kinetics of nucleo-cytoplasmic mRNA export. *Wiley Interdiscip Rev RNA* 1(3):388–401.
28. Shav-Tal Y, et al. (2004) Dynamics of single mRNPs in nuclei of living cells. *Science* 304(5678):1797–1800.
29. Hirata H, et al. (2002) Oscillatory expression of the bHLH factor Hes1 regulated by a negative feedback loop. *Science* 298(5594):840–843.
30. Swinburne IA, Miguez DG, Landgraf D, Silver PA (2008) Intron length increases oscillatory periods of gene expression in animal cells. *Genes Dev* 22(17):2342–2346.
31. Takashima Y, Ohtsuka T, González A, Miyachi H, Kageyama R (2011) Intronic delay is essential for oscillatory expression in the segmentation clock. *Proc Natl Acad Sci USA* 108(8):3300–3305.
32. Chao LC, Jamil A, Kim SJ, Huang L, Martinson HG (1999) Assembly of the cleavage and polyadenylation apparatus requires about 10 seconds in vivo and is faster for strong than for weak poly(A) sites. *Mol Cell Biol* 19(8):5588–5600.
33. Salditt-Georgieff M, Harpold M, Sawicki S, Nevins J, Darnell JE, Jr. (1980) Addition of poly(A) to nuclear RNA occurs soon after RNA synthesis. *J Cell Biol* 86(3):844–848.
34. Morales AV, Yasuda Y, Ish-Horowicz D (2002) Periodic *Lunatic fringe* expression is controlled during segmentation by a cyclic transcriptional enhancer responsive to notch signaling. *Dev Cell* 3(1):63–74.
35. Rabani M, et al. (2011) Metabolic labeling of RNA uncovers principles of RNA production and degradation dynamics in mammalian cells. *Nat Biotechnol* 29(5):436–442.
36. Lei H, Dias AP, Reed R (2011) Export and stability of naturally intronless mRNAs require specific coding region sequences and the TREX mRNA export complex. *Proc Natl Acad Sci USA* 108(44):17985–17990.
37. Rodríguez-Navarro S, Hurt E (2011) Linking gene regulation to mRNA production and export. *Curr Opin Cell Biol* 23(3):302–309.
38. Wright D, et al. (2009) Cyclic *Nrarp* mRNA expression is regulated by the somitic oscillator but Nrarp protein levels do not oscillate. *Dev Dyn* 238(12):3043–3055.
39. Tam PP (1981) The control of somitogenesis in mouse embryos. *J Embryol Exp Morphol* 65(Suppl):103–128.
40. William DA, et al. (2007) Identification of oscillatory genes in somitogenesis from functional genomic analysis of a human mesenchymal stem cell model. *Dev Biol* 305(1):172–186.
41. Forsberg H, Crozet F, Brown NA (1998) Waves of mouse *Lunatic fringe* expression, in four-hour cycles at two-hour intervals, precede somite boundary formation. *Curr Biol* 8(18):1027–1030.
42. McGrew MJ, Dale JK, Fraboulet S, Pourquié O (1998) The *lunatic fringe* gene is a target of the molecular clock linked to somite segmentation in avian embryos. *Curr Biol* 8(17):979–982.
43. Bhatt DM, et al. (2012) Transcript dynamics of proinflammatory genes revealed by sequence analysis of subcellular RNA fractions. *Cell* 150(2):279–290.
44. Stauber M, Laclef C, Vezzaro A, Page ME, Ish-Horowicz D (2012) Modifying transcript lengths of cycling mouse segmentation genes. *Mech Dev* 129(1-4):61–72.
45. Harima Y, Takashima Y, Ueda Y, Ohtsuka T, Kageyama R (2013) Accelerating the tempo of the segmentation clock by reducing the number of introns in the *Hes7* gene. *Cell Rep* 3(1):1–7.
46. Audibert A, Weil D, Dautry F (2002) In vivo kinetics of mRNA splicing and transport in mammalian cells. *Mol Cell Biol* 22(19):6706–6718.
47. Pandya-Jones A, Black DL (2009) Co-transcriptional splicing of constitutive and alternative exons. *RNA* 15(10):1896–1908.
48. Grünwald D, Singer RH (2010) In vivo imaging of labelled endogenous β-actin mRNA during nucleocytoplasmic transport. *Nature* 467(7315):604–607.
49. Mor A, et al. (2010) Dynamics of single mRNP nucleocytoplasmic transport and export through the nuclear pore in living cells. *Nat Cell Biol* 12(6):543–552.
50. Siebrasse JP, Kaminski T, Kubitscheck U (2012) Nuclear export of single native mRNA molecules observed by light sheet fluorescence microscopy. *Proc Natl Acad Sci USA* 109(24):9426–9431.
51. Hirata H, et al. (2004) Instability of Hes7 protein is crucial for the somite segmentation clock. *Nat Genet* 36(7):750–754.
52. Moore MJ, Proudfoot NJ (2009) Pre-mRNA processing reaches back to transcription and ahead to translation. *Cell* 136(4):688–700.
53. Bass J (2012) Circadian topology of metabolism. *Nature* 491(7424):348–356.
54. Warming S, Costantino N, Court DL, Jenkins NA, Copeland NG (2005) Simple and highly efficient BAC recombineering using galK selection. *Nucleic Acids Res* 33(4):e36.
55. Henrique D, et al. (1995) Expression of a *Delta* homologue in prospective neurons in the chick. *Nature* 375(6534):787–790.